A short peptide insertion crucial for angiostatic activity of human tryptophanyl-tRNA synthetase

Yoshiaki Kise[1], Sang Won Lee[2], Sang Gyu Park[2], Shuya Fukai[3], Toru Sengoku[1], Ryohei Ishii[1], Shigeyuki Yokoyama[1,4], Sunghoon Kim[2] & Osamu Nureki[3–5]

Human tryptophanyl-tRNA synthetase (TrpRS) is secreted into the extracellular region of vascular endothelial cells. The splice variant form (mini TrpRS) functions in vascular endothelial cell apoptosis as an angiostatic cytokine. In contrast, the closely related human tyrosyl-tRNA synthetase (TyrRS) functions as an angiogenic cytokine in its truncated form (mini TyrRS). Here, we determined the crystal structure of human mini TrpRS at a resolution of 2.3 Å and compared the structure with those of prokaryotic TrpRS and human mini TyrRS. Deletion of the tRNA anticodon-binding (TAB) domain insertion, consisting of eight residues in the human TrpRS, abolished the enzyme's apoptotic activity for endothelial cells, whereas its translational catalysis and cell-binding activities remained unchanged. Thus, we have identified the inserted peptide motif that activates the angiostatic signaling.

Aminoacyl-tRNA synthetases (aaRSs) catalyze the covalent attachment of amino acids to their cognate tRNAs in the first step of protein synthesis[1]. So far, 20 of the 21 expected aaRS structures have been reported. They are naturally divided into two classes (I and II) based on the architecture of the catalytic domains, with both classes basically composed of a core catalytic domain and an appended tRNA-binding domain. In class I aaRSs, an insertion domain, referred to as CP1, is within the catalytic Rossmann fold. Structural analyses suggest that the various domains have been hierarchically assembled to construct the contemporary aaRS structures, thereby attaining the strict substrate discrimination inherent to their function. Recent biological studies have shown that aaRSs also carry out unexpected functions in other crucial cellular activities, including rRNA processing, RNA splicing, RNA trafficking, transcriptional and translational regulation[2,3], and apoptosis[3,4]. Previous sequence comparisons have shown that mammalian aaRSs have noncatalytic extension domains that are absent from prokaryotic aaRSs. These extension domains are thought to be involved in the assembly of multisynthetase complexes or in other cellular functions[5].

TrpRS is a homodimeric enzyme belonging to class I. The *Bacillus stearothermophilus* TrpRS crystal structure shows a compact domain organization consisting of a catalytic Rossmann fold domain, a CP1 domain involved in molecular dimerization and an α-helical TAB domain[6]. As compared with the prokaryotic enzyme, human TrpRS has an N-terminal extension sequence (residues 1–154), with a portion (residues 12–65) sharing sequence similarity with the

mammal-specific extension-insertion domains of the human histidyl-tRNA, glycyl-tRNA, methionyl-tRNA and prolyl-glutamyl-tRNA synthetases (HisRS, GlyRS, MetRS and ProGluRS, respectively). The insertion motif of ProGluRS adopts a helix-turn-helix structure and has tRNA-binding activity[7]. Notably, this motif has also been identified as an antigenic epitope for autoantibodies in myositis patients[8]. Mammalian TrpRS has long been suspected of carrying out important activities outside of protein synthesis, on the basis of the high-level expression of bovine TrpRS in the pancreas, with its various truncated forms secreted into pancreatic juice[9–12]. The closely related human TyrRS is also released into the extracellular region from apoptotic cells. Polymorphonuclear leukocyte (PMN) elastase cleaves the protein into two cytokines, the C-terminal EMAPII-like domain and the N-terminal catalytic domain, mini TyrRS[13]. Mini TyrRS functions as a chemoattractant for PMN leukocytes by binding to the chemokine receptor CXCR1 and the interleukin-8 (IL-8) receptor, and acts on endothelial cells as an angiogenic cytokine[13,14].

Mini TrpRS, the splice variant form of human TrpRS, lacks the N-terminal 47 residues[15,16]. The expression of mini TrpRS is suppressed in normal cells but is highly stimulated *in vitro* by interferon-γ (IFN-γ), which is responsible for the antiviral and antiproliferative states of animal cells[12,15,17,18]. IFN-γ also induces expression of the CXC chemokines IP-10 (IFN-inducible protein 10) and Mig (monokine induced by IFN-γ), which are typically associated with T$_H$1 responses and are highly expressed in several inflammatory skin conditions. IP-10 and Mig are angiostatic (antiangiogenic)

[1]Department of Biophysics and Biochemistry, Graduate School of Science, the University of Tokyo, 7-3-1 Hongo, Bunkyo-ku, Tokyo 113-0033, Japan. [2]National Creative Research Initiatives Center for ARS Network, College of Pharmacy, Seoul National University, Seoul 145-742, Korea. [3]Department of Biological Information, Graduate School of Bioscience and Biotechnology, Tokyo Institute of Technology, 4259 Nagatsuta-cho, Midori-ku, Yokohama-shi, Kanagawa 226-8501, Japan. [4]RIKEN Genomic Sciences Center, 1-7-22 Suehiro-cho, Tsurumi, Yokohama 230-0045, Japan. [5]PRESTO, Japan Science and Technology. Correspondence should be addressed to O.N. (onureki@bio.titech.ac.jp) or S.K. (sungkim@snu.ac.kr).

a

b
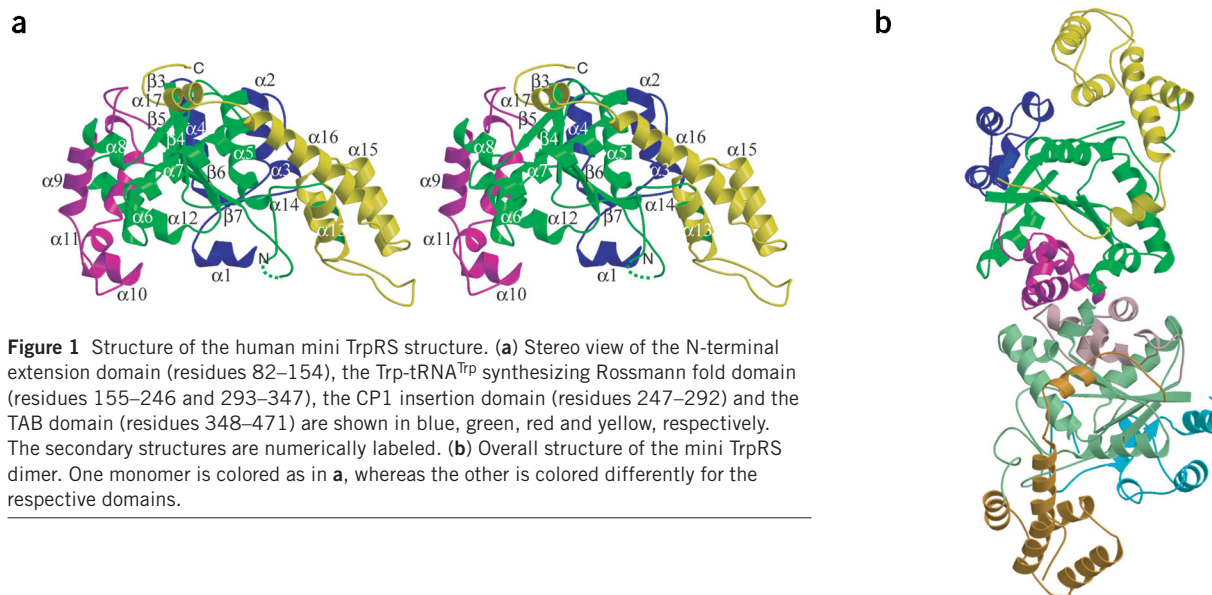
Figure 1 Structure of the human mini TrpRS structure. (**a**) Stereo view of the N-terminal extension domain (residues 82–154), the Trp-tRNA^{Trp} synthesizing Rossmann fold domain (residues 155–246 and 293–347), the CP1 insertion domain (residues 247–292) and the TAB domain (residues 348–471) are shown in blue, green, red and yellow, respectively. The secondary structures are numerically labeled. (**b**) Overall structure of the mini TrpRS dimer. One monomer is colored as in **a**, whereas the other is colored differently for the respective domains.

chemokines, in contrast to other CXC chemokines, such as IL-8, that promote angiogenesis. It was recently demonstrated that human mini TrpRS inhibits VEGF-induced or mini TyrRS-induced angiogenesis[14,16]. Thus, the two closely related enzymes, human TyrRS and TrpRS, have opposite cytokine activities in angiogenesis[13,14,16,19,20]. Furthermore, the full-length TrpRS lacks angiostatic activity[16], indicating that truncation of the N-terminal domain is required for expression of this particular function.

The crystal structures of the eubacterial TrpRS[6] and the human mini TyrRS[21] have been reported. However, the eukaryotic TrpRS structure has not been solved, and the structural basis for the angiostatic activity of mini TrpRS remains unknown. Here we determined the crystal structure of human mini TrpRS at a resolution of 2.3 Å. We compared the human mini TrpRS structure with those of eubacterial TrpRS and human mini TyrRS, and carried out functional analyses using a series of deletion mutants of the mini TrpRS. These analyses revealed the structural motif crucial for the cytokine activity of TrpRS and provided a structural basis for the opposite cytokine activities of mini TrpRS and mini TyrRS.

RESULTS
Overall structure
Human mini TrpRS, a splice variant form, is a dimer (424×2 residues with a relative molecular mass of 96 kDa). The present model at a

resolution of 2.3 Å comprises residues 82–471 in the A subunit and residues 100–471 in the B subunit (hereafter, residue numbering is based on full-length TrpRS) (**Fig. 1**). TrpRS exhibits the typical class I aaRS structural features and contains four domains. Residues 82–154 (**Fig. 1a**) fold into the N-terminal extension domain, which is unique to human TrpRS and is absent in prokaryotic enzymes. Residues 48–81 in the A subunit and residues 48–99 in the B subunit are structurally disordered. Residues 155–347 (**Fig. 1a**) form Rossmann fold nucleotide-binding domain, which catalyzes Trp-tRNA^{Trp} synthesis. The CP1 domain (residues 247–292, **Fig. 1a**) intervenes within the Rossmann fold domain. Residues 348–471 (**Fig. 1a**) may form the TAB domain, as suggested by similarities to the TyrRS–tRNA complex structures[22,23]. In addition to the disorder in the N-terminal extension domain, the KMSAS catalytic loop is structurally disordered in the A subunit, whereas residues 381–392 in the TAB domain and residues 470–471 are disordered in the B subunit. The two mini TrpRS monomers dimerize at the hydrophobic interface of the CP1 domain, as observed in eubacterial TrpRS[6] (**Fig. 1b**).

Structural comparison with prokaryotic TrpRS
The overall structures of human TrpRS and eubacterial *B. stearothermophilus* TrpRS[6] are quite similar (**Fig 2a,b**). Superimposition of 100 Cα atoms in the Rossmann fold domain gave an r.m.s. deviation of 1.66 Å, whereas superimposition of the TAB

a

b

c
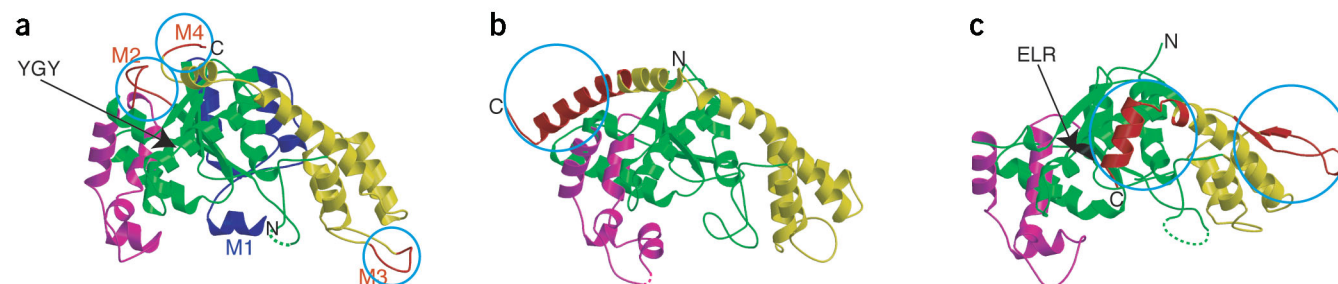
Figure 2 Structural comparison. (**a**) Human mini TrpRS. (**b**) *B. stearothermophilus* TrpRS. (**c**) human mini TyrRS. Color coding is as in **Figure 1a**. The unique structural features in each protein are circled. The TrpRS-specific structures are indicated as M1, M2, M3 and M4. The YGY sequence of mini TrpRS and the ELR motif of mini TyrRS are indicated.

domains gave an r.m.s. deviation of 2.27 Å (79 Cα atoms). However, the two domains cannot be simultaneously superimposed, because the orientations of the two domains differ considerably between the two TrpRSs.

Although their overall structures are similar, human mini TrpRS contains unique structures as compared with *B. stearothermophilus* TrpRS (**Fig. 2a,b**). The first of these structures is an extended N-terminal helical domain composed of residues 82–154 (designated M1 in **Fig. 2a**). The next unusual feature of mini TrpRS is an inserted loop structure (residues 293–304, designated M2 in **Fig. 2a**) in the CP1 domain. The presence of this inserted loop causes the C termini of the human and eubacterial TrpRSs to be oriented quite differently. As a result, the long C-terminal helix forms part of the dimer interface in *B. stearothermophilus* TrpRS. In contrast, the C-terminal helix is short and uninvolved in subunit dimerization in human mini TrpRS, and folds back toward the TAB domain (designated M4 in **Fig. 2a**). The other chief difference between the two TrpRS structures is the insertion of a loop formed by residues 381–390 in the TAB domain (designated M3 in **Fig. 2a**) of mini TrpRS. Nine of the ten amino acid residues in this insertion loop are strictly conserved among mammalian TrpRSs (see **Supplementary Fig. 1** online). As suggested by sequence alignments, the archaeal and yeast TrpRSs contain comparable insertions that share only limited sequence homology with the mammalian enzymes (see **Supplementary Fig. 1** online). Despite the considerable overall similarity of the human mini and *B. stearothermophilus* TrpRS structures, only the former exhibits angiostatic cytokine activity. This suggests that either one or a few of the unique human mini TrpRS structures, the N-terminal extension domain, the two insertion loops and the C terminus, may function in its cytokine activity.

Mini TrpRS in turn lacks some structures seen in *B. stearothermophilus* TrpRS. These structures include residues Thr106–Ser112 in the CP1 domain and residues Asp231–Gly237 in the anticodon-binding domain (residue numbering based on *B. stearothermophilus* TrpRS). Intriguingly, these regions have been suggested to be involved in tRNA recognition by bacterial TrpRS, on the basis of computer modeling and mutational analyses[24]. In contrast, residues 83–92 in mini TrpRS, which form an antiparallel β-sheet in the B subunit, are located close to the KMSAS catalytic loop. This suggests that the disordered N-terminal extension domain may interact with tRNA in mini TrpRS. This is supported by the finding that the N-terminal extension domain of mammalian HisRS, which is highly homologous to the N-terminal extension of TrpRS, is essential for tRNA recognition[25].

Structural comparison with mini TyrRS

Human mini TyrRS is an angiogenic cytokine, whereas human mini TrpRS is an angiostatic cytokine[14,18,20]. Despite the opposing functions of human mini TrpRS and TyrRS[20], their overall structures are markedly similar, with an r.m.s. deviation of 1.43 Å by superposition of 120 Cα atoms of the Rossmann fold domain (**Fig. 2a,c**). However, several differences are noticeable between these two closely related synthetases. These differences are the same as those mentioned earlier between human mini TrpRS and *B. stearothermophilus* TrpRS. In the TAB domain insertion (M3, **Fig. 2a**) of mini TrpRS, mini TyrRS instead has a hairpin structure, consisting of an antiparallel β-sheet, which is inserted closer to the C-terminal side (**Fig. 2c**). These structural differences may contribute to tRNA recognition or binding with their respective receptors, providing a basis on which the two proteins exhibit their opposing cytokine activities.

In mini TyrRS, the Glu91-Leu92-Arg93 (ELR) motif in the Rossmann fold domain is essential for receptor binding[13] (**Fig. 2c**). On
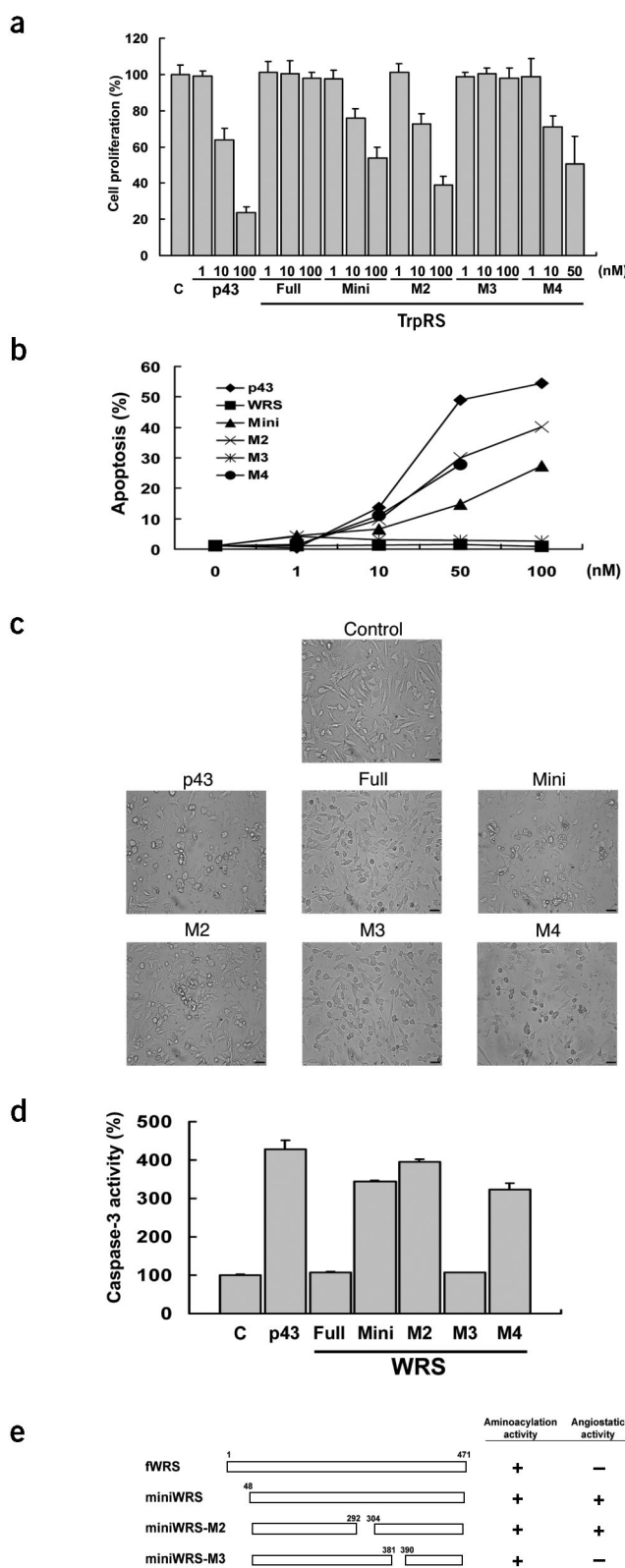
Figure 3 *In vitro* apoptotic activities and housekeeping translational activities of TrpRS mutants. (**a**) The effect of the TrpRS deletion mutants on the proliferation of BAECs. (**b**) Effect of the TrpRS deletion mutants on BAEC apoptosis. (**c**) Representative images of apoptotic cell morphology, in treatments with p43 and TrpRS mutants. Scale bar, 100 μm. (**d**) The activation of caspase-3 by TrpRS deletion mutants. (**e**) Summary of the aminoacylation and angiostatic activities of the TrpRS mutants.

a

b
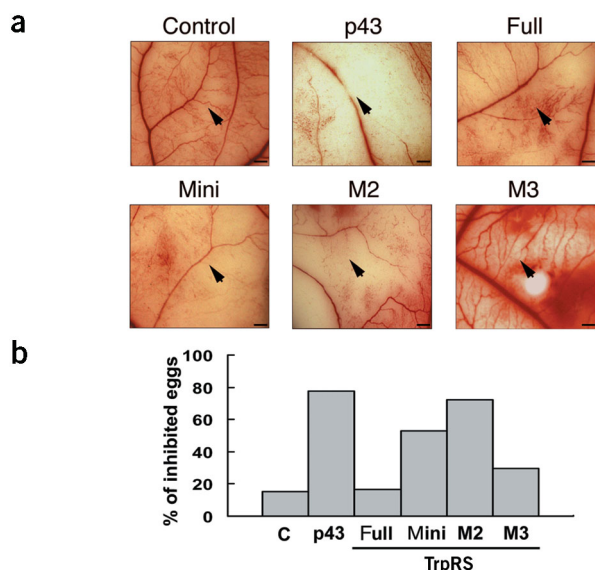
Figure 4 Angiogenesis assay in chick CAM. (**a**) Photographic images of *in vivo* angiogenesis assay in CAM. The arrows indicate the point at which the p43- and TrpRS-treated coverslips were loaded onto the CAM of the developing eggs. Scale bar, 200 µm. (**b**) A quantitative evaluation of the angiostatic activity. The p43 was used as a positive control.

induced apoptosis of BAECs, whereas M3 again did not, as determined by the apoptotic cell morphology (**Fig. 3b,c**) and the activation of caspase-3 (**Fig. 3d**). The M4 mutant showed antiproliferative and proapoptotic activities similar to those of mini TrpRS and M2, although the low solubility of M4 prevented us from testing its activity over the full concentration range used for the other mutants (**Fig. 3a–d**). In contrast, the full-length TrpRS (negative control) and the M3 mutant were inactive in both assays (**Fig. 3**). These results indicate that the eight-residue (D382-TIEEHR-Q389) TAB domain insertion loop of mini TrpRS has a crucial role in its angiostatic activity. None of the deletion mutants showed reduced housekeeping aminoacylation activities, as compared with those of the full-length and mini TrpRSs (**Fig. 3e**).

To confirm the effects of the mutants on *in vivo* angiogenesis, we conducted an angiogenesis assay using chick chorioallantoic membranes (CAM). Whereas the mini and M2 TrpRSs as well as p43 (positive control) inhibited CAM angiogenesis, the full-length TrpRS and

the basis of the present structural comparison, the ELR motif is replaced by Tyr212-Gly213-Tyr214 (YGY) in human mini TrpRS (**Fig. 1c** and **Supplementary Fig. 1** online). Whereas the glycine in the YGY sequence is replaced by serine in the mouse, the two tyrosine residues are strictly conserved in all mammals (see **Supplementary Fig. 1** online). Therefore, these two tyrosine residues in mini TrpRS may be involved in receptor binding and could control the activity of mini TrpRS.

The inserted motif is essential for apoptosis

We constructed four deletion mutants, each lacking a particular structure unique to human TrpRS. The structures removed from human TrpRS were the N-terminal extension domain (residues 48–153 (M1)), the insertion loops in the CP1 and TAB domains (residues 293–303 (M2) and 382–389 (M3), respectively) and the C-terminal region (residues 466–471 (M4)). Whereas M2 and M3 were soluble, M1 was extremely insoluble. Although M4 also showed very low solubility, we purified a sufficient quantity of the soluble form to determine its activity.

To determine whether the mutants M2, M3 and M4 had angiostatic activity, we first tested their effects on the proliferation and death of endothelial cells. Bovine aorta endothelial cells (BAECs) were treated with each of the mutants, and cell proliferation was monitored by the incorporation of [^{3}H]thymidine. The wild-type (mini) TrpRS and M2 mutant both suppressed cell proliferation to ~50–60% of that of the control cells in a dose-dependent manner, whereas the M3 mutant and the full-length TrpRS did not (**Fig. 3a** and data not shown). The mammalian aaRS-associating factor p43, which has angiostatic activity[26], was used as a positive control. Mini TrpRS and the M2 mutant also

a

b
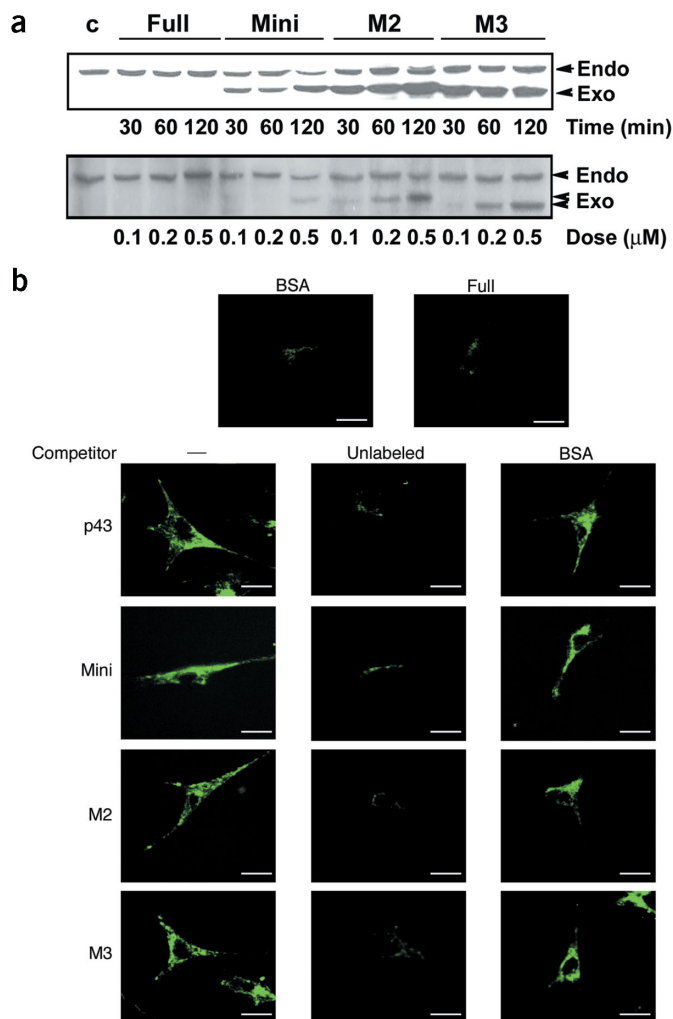
Figure 5 Binding of the TrpRS deletion mutants to BAECs. (**a**) Top, BAECs were treated with 0.5 µM of wild type and mutant TrpRSs for 30, 60 or 120 min, respectively. Bottom, the indicated amount of each TrpRS deletion mutant was incubated with BAECs for 60 min. TrpRS binding to BAECs was determined by immunoblotting with a polyclonal antibody to TrpRS. Endo and Exo represent endogenously generated and exogenously added TrpRSs, respectively. (**b**) Biotin-labeled TrpRS binding to BAECs. To address the cell-binding specificity, biotin-labeled TrpRSs were challenged with a 20-fold molar excess of unlabeled TrpRSs and BSA. Top panels, biotin-labeled BSA and full-length TrpRS not binding to BAECs (negative control). Scale bar, 25 µm.

M3 mutant did not (**Fig. 4a**). These results, together with those described earlier, strongly suggest that the eight-residue loop inserted within the TAB domain of mini TrpRS is involved in the activation of apoptotic signaling *in vitro* and *in vivo*. The angiostatic activity of the M2 mutant was more pronounced than that of mini TrpRS in both the *in vivo* (**Fig. 4a,b**) and *in vitro* assays (**Fig. 3**).

Cell-binding activity

To determine how the M3 mutant lost its cytokine activity, we studied its ability to bind endothelial cells. Although both the mini TrpRS and M2 mutant bound to the cells in time- and dose-dependent manners, the latter showed higher cell-binding affinity (**Fig. 5a**), implying that the deletion of residues 293–303 results in increased cell binding and angiostatic activity. The binding of TrpRS to the receptor does not seem directly related to its cytokine activity, as the M3 mutant (which lacks cytokine activity) also binds to the cells at a higher rate and affinity than does mini TrpRS (**Fig. 5a**). The specific binding of mini TrpRS and the M2 and M3 mutants to BAECs was further supported by microscopic imaging using fluorescently labeled TrpRSs (**Fig. 5b**).

Mutation of the YGY motif

To study the function of the YGY motif of human TrpRS, we prepared two mutants in which the two tyrosine residues were replaced with phenylalanine or alanine (FGF and AGA mutants, respectively). Both of these mutants were extremely insoluble and could not be used for activity determination assays. We then mutated the YGY sequence to ELR, the corresponding motif found in human mini TyrRS. Although this mutant was also relatively insoluble, we purified an adequate amount for activity determinations. Even with this drastic mutation, the ELR mutant showed normal apoptotic activity for BAECs, comparable to that of the wild-type mini TrpRS (**Fig. 6a,b**). When we further deleted the eight-residue loop insertion in the TAB domain of the ELR mutant—referred to as the M3 (ELR) mutant—the apoptotic activity was lost (**Fig. 6c**). Nonetheless, the M3 (ELR) mutant still retained the same cell-binding activity as the M3 mutant (**Fig. 6d**). These results indicate that the YGY sequence does not solely determine the cell-binding and angiostatic activities of mini TrpRS. The YGY sequence of mini TrpRS, like the ELR motif of TyrRS, is located on an α-helix (α7 in mini TrpRS, **Fig. 1a**) that is exposed on the protein surface (**Fig. 2a,c**). In contrast, the ELR motifs of the ELR$^+$ CXC chemokines, such as IL-8 (see below), are located within the N-terminal flexible loop. The first tyrosine residue in the YGY sequence provides hydrogen-bonding and hydrophobic interactions on the protein surface, whereas the second tyrosine enters an inside pocket, where it may stabilize the protein structure. This may explain why the protein became insoluble when certain replacements were introduced into the YGY motif.

DISCUSSION

The noncanonical functions of eukaryotic aaRSs have long been attributed to their unique N-terminal or C-terminal extension domains. We found that the N-terminal extension of TrpRS actually has negative roles, in both its endothelial cell–binding and its angiostatic activities. The present study revealed that the eight-residue loop insertion in the TAB domain is required for the angiostatic cytokine activity of human TrpRS. The absence of this inserted peptide abolished the apoptotic activity for vascular endothelial cells, but the housekeeping tRNA aminoacylation activity remained unaffected, demonstrating the independence of the two functions. Notably, the deletion of this peptide enhanced the cell binding (**Fig. 5a**). Perhaps the structure around the receptor-binding site of
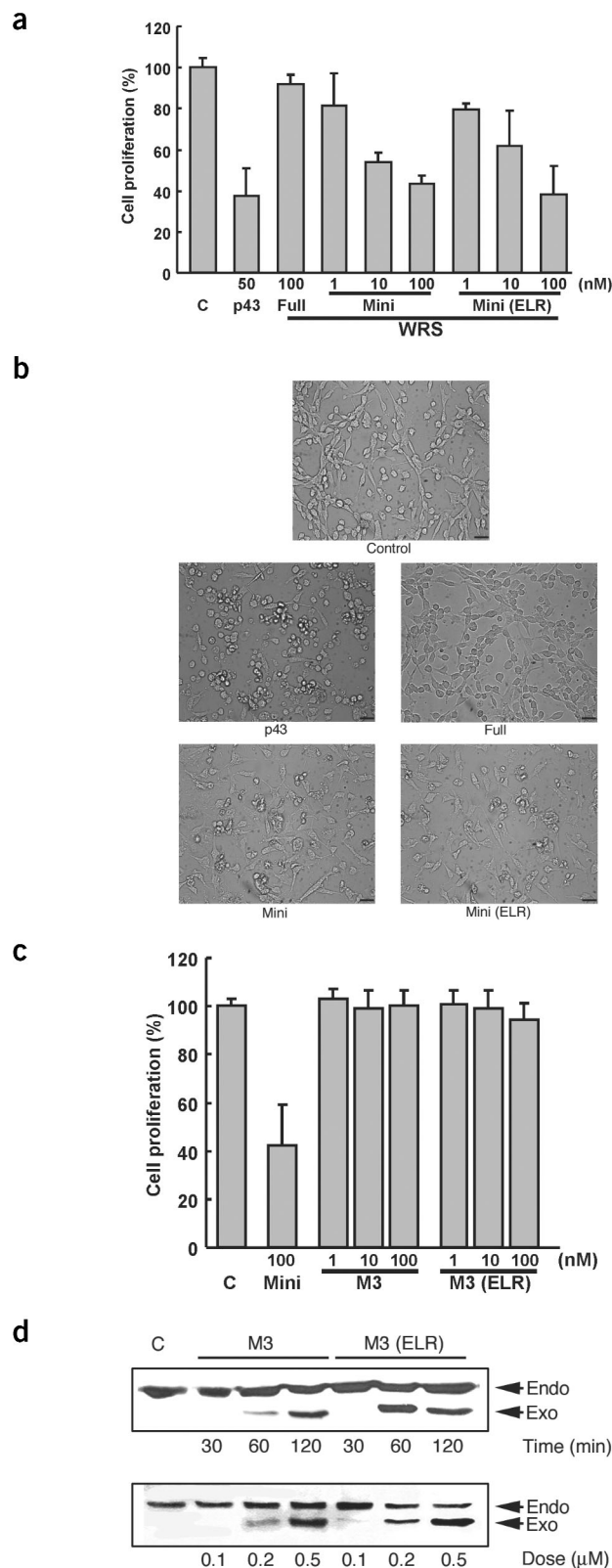
Figure 6 The effect of the YGY sequence mutation on the proliferation of BAECs and cell binding. (**a**) BAEC proliferation activities of mini TrpRS and the ELR mutant. (**b**) Images of apoptotic cell morphology in treatments with mini TrpRS and the mini TrpRS(ELR) mutant. Scale bar, 100 μm. (**c**) BAEC proliferation activities of the M3 mutant and M3 (ELR) mutants. (**d**) BAEC binding activities of the M3 and M3 (ELR) mutants.

Table 1 Data collection, phasing and refinement statistics

	Peak	Edge	Remote (low)	Remote (high)
Data collection				
Wavelength (Å)	0.9797	0.9799	0.9843	0.9734
Resolution (Å)	50–2.3	50–2.3	50–2.3	50–2.3
Total reflections	108,511	106,623	103,600	92,810
Redundancy	2.7	2.6	2.6	2.4
Completeness (%)[a]	91.0 (77.9)	90.1 (76.4)	89.1 (72.2)	86.3 (68.5)
$I / \sigma (I)$[a]	21.1 (2.8)	20.6 (2.3)	19.8 (2.1)	17.2 (1.7)
R_{sym} (%)[a,b]	7.3 (19.9)	5.6 (21.5)	5.4 (23.1)	6.8 (25.7)
Phasing statistics				
No. of sites	16	16	16	16
Phasing power				
Acentric	0.20	–	0.95	0.79
Centric	0.17	–	0.76	0.67
R_{cullis}[c]				
Isomorphous				
Acentric	0.99	–	0.86	0.87
Centric	0.98	–	0.76	0.79
Anomalous	0.71	0.83	0.94	0.79
Figure of merit				
Acentric	0.48			
Centric	0.47			
Refinement				
Resolution (Å)	50–2.3			
Reflections	38,683			
Protein atoms	6,014			
Water molecules	477			
[d]R_{work} (%)	22.9			
[e]R_{free} (%)	29.1			
R.m.s. deviations				
Length(Å)	0.0073			
Angles (°)	1.41			
Dihedrals (°)	21.51			
Impropers (°)	0.90			

[a]Values in parentheses are for the highest-resolution shell. [b]$R_{sym} = \Sigma |I_{avg} - I_i| / \Sigma I_i$. [c]$R_{cullis} = \Sigma ||F_{PH} + F_P| - F_H(calc)| / \Sigma |F_{PH}|$. [d]$R_{work} = \Sigma|F_o - F_c| / \Sigma F_o$ for reflections of work set. [e]$R_{free} = \Sigma|F_o - F_c| / \Sigma F_o$ for reflections of test set (10% of total reflections).

mini TrpRS is changed by the deletion of this motif, allowing it to bind to the receptor more easily, but unproductively. Alternatively, the TAB domain insertion loop may have a switching role in activating the apoptotic signal, with the actual receptor-binding sites located elsewhere in the mini TrpRS structure. A clear answer warrants further detailed investigation.

Mini TrpRS inhibits the angiogenesis induced not only by mini TyrRS, but also by VEGF and the ELR[+] chemokine IL-8. Mini TyrRS also has an ELR motif and binds to a chemokine receptor, CXCR1, which is a common feature of the ELR[+] CXC chemokines[13]. In contrast, VEGF binds to a different receptor, VEGFR. Considering that mini TrpRS inhibits both of the angiogenic factors that bind distinct receptors, it is reasonable to propose that TrpRS does not block the receptor binding of mini TyrRS, IL-8 and VEGF by competition, but that it binds its own cognate receptor, which inhibits angiogenesis by intracellular signaling after ligand binding. IFN-γ induces the expression of other angiostatic chemokines, such as IP-10 and Mig, as well as mini TrpRS. IP-10 and Mig inhibit IL-8–induced angiogenesis, whereas IP-10 further inhibits the angiogenic activity of mini TyrRS.

IP-10 and Mig are ELR[−] chemokines, but except for this point, IL-8 and IP-10 have very similar structures[27]. Whereas IL-8 binds to CXCR1 and induces angiogenesis, IP-10 and Mig bind to CXCR3 and inhibit IL-8 activity. Considering that IL-8 and mini TyrRS, which both bind the CXCR1 receptor, share structural similarities with IP-10 and mini TrpRS, respectively, we speculate that mini TrpRS binds to the CXCR3 receptor, as does IP-10. CXCR3 is expressed not only in T_H1 cells but also in vascular endothelial cells[28]. A preliminary sequence alignment revealed that the inserted peptide in the TrpRS TAB domain, which we found to be involved in apoptotic signaling, shares sequence similarity with Mig and IP-10 near the putative receptor-binding site[27] (data not shown).

The inserted peptide forms a characteristic turn that exposes four charged residues (see **Supplementary Fig. 2** online). Previous mutagenesis studies[27] on chemokines and their receptors have shown that receptor binding and activation can be separated in terms of a two-step binding mechanism: the first binding step involves hydrophobic interactions between the chemokine and the receptor for receptor recognition, and the second step is charge-mediated and may switch the receptor to an active form. In IL-8, the mutation of the ELR motif near the N terminus severely affected receptor activation but only modestly affected on receptor binding. Here we suggest a similar role for the TAB domain insertion, which may provide charge-mediated interactions for receptor activation but is not essential for initial binding. We could not disregard the possibility that mini TrpRS acts as an antagonist to the CXCR1 receptor, as a result of the structural similarity of the E386-H387-R388 portion to the ELR motif of IL-8. The TAB domain insertion loop is spatially sequestered from the other domain but has several interactions with the TAB domain. Considering that the deletion of the inserted peptide affected neither tRNA aminoacylation nor receptor-binding activity, we conclude that the eight-residue motif is directly involved in the angiostatic activity of mini TrpRS. The weak electron density of the N-terminal disordered region stretches toward the TAB domain, suggesting that the N-terminal domain of full-length TrpRS may mask the TAB domain insertion, thereby preventing mini TrpRS from activating the angiostatic receptor (data not shown). In contrast, our experimental results suggest that, whereas the YGY sequence of human TrpRS is structurally analogous to the ELR motif of mini TyrRS, YGY is not essential for the angiostatic or cell-binding activities but instead is important for structural stability.

It remains to be explained when and how mini TrpRS is secreted in the extracellular region and inhibits angiogenesis *in vivo*. For human mini TyrRS, the full-length protein is secreted from apoptotic cells and is split by extracellular proteases such as PMN elastase[13] into two distinct proapoptotic cytokines, mini TyrRS and the EMAPII-like cytokine. These cytokines are chemoattractants for PMN leukocytes or monocytes[13]. The expression of human TrpRS is strongly induced by IFN-γ, which is secreted by T_H1 cells. IFN-γ activates macrophages and increases MHC protein expression in the inflammatory response, thereby helping to fight infection and heal wounds. These facts suggest that mini TrpRS might also be secreted from apoptotic cells in tissues during an inflammatory response. Mini TrpRS may be secreted at a late apoptotic state to terminate inflammation by attenuating the angiogenesis induced by mini TyrRS, VEGF and other angiogenic factors. Because abnormal angiogenesis is involved in many pathogenic processes, such as tumorigenesis and ischemia, the accurate positive and negative control of this process would have many useful biomedical applications. Studies on the inhibition of abnormal ocular angiogenesis have been reported using truncated forms of TrpRS, suggesting the potential of this enzyme

cytokine as a therapeutic agent[19,29]. Further advances in the clarification of the structure-function relationship of mini TrpRS may facilitate the design of TrpRS forms that can be used in therapy to treat abnormal angiogenesis and cancer.

METHODS

Protein expression, purification and crystallization. The sequence encoding residues 48–471 of human TrpRS (mini TrpRS) was subcloned into pET26b (Novagen) and overexpressed in *Escherichia coli* BL21 (DE3) codon+ (native) or B834 (DE3) (Se-Met derivative) by induction with 0.5 mM IPTG at 20 °C for 20 h. Cells were harvested, lysed by sonication in buffer A (50 mM Tris-HCl, pH 8.0, 500 mM NaCl, 0.1 mM PMSF and 1 mM DTT) and centrifuged (12,000*g*). The supernatant was filtered and loaded onto a Ni^{2+}-charged HiTrap chelating column (Amersham Biosciences) equilibrated with buffer A. After washing with buffer A including 60 mM imidazole, a linear gradient of imidazole (60–500 mM) was applied to elute the protein. The pooled fractions were dialyzed against buffer B (20 mM Tris-HCl, pH 8.0, and 1 mM DTT), loaded onto a UnoS column (BioRad) equilibrated with buffer B and eluted with a linear gradient of NaCl (0–500 mM). The pooled fractions were concentrated to ~10 mg ml^{-1} with a VivaSpin concentrator (Viva Science), and the buffer was exchanged to 10 mM Tris-HCl, pH 7.4, 50 mM NaCl and 1 mM DTT. The C-terminal His$_6$-tag was not removed. Crystals of native mini TrpRS were obtained by hanging-drop vapor diffusion at 4 °C, after mixing 1 μl of protein solution with an equal volume of reservoir solution containing 100 mM Bis-Tris, pH 5.5, 80–100 mM ammonium acetate and 8–12% (w/v) PEG 10,000. Se-Met derivative crystals were obtained with a reservoir solution containing 100 mM Bis-Tris, pH 6.2, 200 mM ammonium acetate and 12% (w/v) PEG 10,000.

Data collection and structure determination. Crystals were harvested in a buffer containing 110 mM Bis-Tris, pH 5.5, 110 mM ammonium acetate and 16% (w/v) PEG 10,000 (for native) or 110 mM Bis-Tris, pH 6.2, 220 mM ammonium acetate and 16% (w/v) PEG 10,000 (for Se-Met derivative). After supplementation with glycerol as cryoprotectant, the crystals were flash-frozen in liquid nitrogen. Diffraction data of the native and Se-Met derivative crystals were collected at the SPring-8 beamline BL41XU (Harima, Japan). Data were integrated using DENZO[30] and scaled with SCALEPACK[30]. The native and Se-Met derivative crystals belong to space group *C*2 (*a* = 135.21 Å, *b* = 96.55 Å, *c* = 97.64 Å, β = 130.25° for the native crystal, and *a* = 135.87 Å, *b* = 96.50 Å, *c* = 98.23 Å, β = 130.25° for the Se-Met derivative crystal). The structure was determined by MAD. After searching for the sites of Se atoms using SnB[31], phases were determined using MLPHARE[32] at a resolution of 2.5 Å, and then phase extension was done using density modification at a resolution of 2.3 Å. RESOLVE[33] and REFMAC[33] were used for electron-density modification and automodeling. As a result, 393 of 848 residues were successfully automodeled. Model building of the remaining residues was done manually using O[34]. Model refinement was done using CNS[35], and gave an *R*-factor of 24.1% with an R_{free} of 29.2% (**Table 1**). A Ramachandran analysis showed that 87.7%, 10.4% and 1.1% of residues are in the most favored and allowed regions. Disordered regions in the A subunit are residues 48–99 and 347–354. In subunit B, they are residues 48–82, 382–390 and 423–424.

Construction of TrpRS and mutant plasmids. The DNA fragments encoding the deletion (mini, M1–4) and substitution (ELR, FGF and AGA) mutants of TrpRS were generated by three PCR steps and were inserted into the *Nde*I and *Xho*I sites of pET-28a. Primer sequences are available upon request.

BAEC proliferation. BAECs (5 × 10³ cells) were cultured in 24-well plates for 12 h and then treated with p43 and the different TrpRS forms at the indicated concentrations for 16 h. A 1-μCi aliquot of [³H]thymidine was added to each well, and incubation was continued for 4 h. The cells were washed three times with 1× PBS, fixed with 5% (v/v) trichloroacetic acid (TCA), washed again three times with 1× PBS and lysed with 0.5 M NaOH for 30 min at room temperature. The cells incorporating thymidine were counted using a liquid scintillation counter. Three independent experiments were done.

Apoptosis and caspase assays. BAECs (2 × 10⁵ cells) were cultured in DMEM containing 20% (v/v) FBS and 1% (v/v) antibiotics for 12 h, and then were treated with the indicated concentrations of p43 and TrpRSs for 16 h. The apoptotic cells were counted according to their morphology. Errors were within 10% between triplicate assays and two independent experiments. BAECs (2 × 10⁶ cells) were treated with 100 nM of p43 and TrpRS mutants (M4 = 50 nM) for 16 h in DMEM containing 20% (v/v) FBS and 1% (v/v) antibiotics, and were lysed with 300 μl of chilled cell lysis buffer (20 mM HEPES, pH 7.5, 1 mM DTT, 0.1 mM EDTA, 0.5% (v/v) NP-40 and 0.1 mM PMSF). The cell lysates were centrifuged at 14,000 r.p.m. (26,000*g*) for 10 min at 4 °C, and the supernatant fractions were used to measure the caspase-3 activity. The protein extracts (40 μg) of the cell lysates were incubated for 2 h at 30 °C in 20 mM HEPES, pH 7.5, 2 mM DTT and 10% (v/v) glycerol, and 100 μM caspase-3 substrate, Ac-DEVD-*p*-nitroanilide. The amount of *p*-nitroanilide released by the caspase activation was quantified by the optical density at 405 nm. The experiment was repeated twice. For the *in vivo* angiogenesis assay in CAM, coverslips treated with p43 and TrpRS (2 μg) were loaded onto the CAM of the developing eggs, and the antiangiogenic effects of the TrpRSs were monitored.

TrpRS binding to BAECs. BAECs (5 × 10⁶ cells) were cultured at 37 °C on 100-mm dishes to 90% confluency in DMEM containing 20% (v/v) FBS and 1% (v/v) antibiotics. TrpRS and its mutants were added at the indicated concentrations, and the cells were washed twice with 1× PBS and lysed with 50 mM HEPES containing 150 mM NaCl, 10% (v/v) glycerol, 1 mM EDTA, 1 mM PMSF, 1 mM DTT and 1% (v/v) NP-40. Cell lysates were centrifuged at 14,000 r.p.m. (26,000*g*) for 15 min at 4 °C. The supernatants were harvested, and 40 μg of protein from each lysate was resolved by 10% (w/v) SDS-PAGE. After transfer to a PVDF membrane, the TrpRS was detected with anti-TrpRS. The experiment was repeated three times.

To label the TrpRS proteins with biotin, a 20-fold molar excess of biotin was added to each TrpRS mutant in PBS, and the mixture was incubated for 2 h on ice. An aliquot (1/20 volume) of 2 M Tris-HCl (pH 7.4) was added to stop the reaction, and the free biotin was removed by passing the proteins through a desalting column (PD-10, Pharmacia). BAECs (5 × 10⁴ cells) were seeded onto 12-well dishes containing 9 × 9 mm slides, and were cultured in DMEM medium containing 20% (v/v) FBS and 1% (v/v) antibiotics for 12 h. The cells were treated with the biotin-labeled TrpRS mutants, p43 and BSA (50 nM) for 30 min. Cells were fixed with 5% (v/v) formalin for 10 min, and were washed three times with PBS. The cells were permeabilized with 0.1% (v/v) Triton X-100 for 5 min and were washed three times with PBS. The slides were incubated with 1% (v/v) FBS in PBS for 1 h to inhibit the nonspecific binding, and then the biotin-labeled TrpRSs were captured with FITC-conjugated streptavidin. Biotin-labeled TrpRS was visualized by confocal microscopy (60×). To determine whether the cell binding was specific, 1 μM concentrations of each unlabeled TrpRS and BSA were used to compete for binding with 50 nM of the biotin-labeled TrpRSs.

Aminoacylation assay. TrpRS and the mutants were overexpressed as His$_6$-tagged proteins in *E. coli* BL21 (DE3), and were purified using nickel affinity chromatography following the manufacturer's protocol (Qiagen). To remove the lipopolysaccharide (LPS), the protein solutions were dialyzed in pyrogen-free buffer (10 mM potassium phosphate buffer, pH 6.0, and 100 mM NaCl). The protein solutions were then loaded onto a polymyxin resin (Bio-Rad) pre-equilibrated with the same buffer, incubated for 20 min and eluted. To remove the residual LPS, the protein solutions were dialyzed against PBS containing 20% (v/v) glycerol and then filtered with a Posidyne membrane (Pall Corporation).

The aminoacylation reaction was carried out using *E. coli* total tRNA as the substrate. The reaction mixture contained 50 mM HEPES, pH 7.5, 25 mM MgCl₂, 20 mM KCl, 20 mM β-mercaptoethanol, 200 μg ml^{-1} BSA, 5 mM ATP, 100 μM [³H]tyrosine (specific activity, 100 mCi mmol^{-1}) and 10 mg ml^{-1} *E. coli* total tRNA. The reaction was initiated at 37 °C by the addition of 10 nM of each enzyme. Aliquots of the reactions were taken at various time intervals and were quenched by 10% (v/v) TCA on filter paper (Whatman, 3MM, UK). After washing the filter paper, the amount of tRNA charged with the radioactive tryptophan was measured with a liquid scintillation counter (LKB).

Coordinates. Coordinates and structure factors have been deposited in the Protein Data Bank (accession code 1ULH).

ARTICLES

1. Ibba, M. & Soll, D. Aminoacyl-tRNA synthesis. *Annu. Rev. Biochem.* **69**, 617–650 (2000).
2. Martinis, S.A., Plateau, P., Cavarelli, J. & Florentz, C. Aminoacyl-tRNA synthetases: a family of expanding functions. *EMBO J.* **18**, 4591–4596 (1999).
3. Ko, Y.G., Park, H. & Kim, S. Novel regulatory interactions and activities of mammalian tRNA synthetases. *Proteomics* **2**, 1304–1310 (2002).
4. Ko, Y.G. *et al*. Glutamine-dependent antiapoptotic interaction of human glutaminyl-tRNA synthetase with apoptosis signal-regulating kinase 1. *J. Biol. Chem.* **276**, 6030–6036 (2001).
5. Kisselev, L.L. & Wolfson, A.D. Aminoacyl-tRNA synthetases from higher eukaryotes. *Prog. Nucleic Acids Res. Mol. Biol.* **48**, 83–142 (1994).
6. Doublie, S., Bricogne, G., Glimore, C. & Carter, C. Tryptophanyl-tRNA synthetase crystal structure reveals an unexpected homology to tyrosyl-tRNA synthetase. *Structure* **3**, 17–31 (1995).
7. Jeong, E.S. *et al*. Structural analysis of peptide motifs in human bifunctional tRNA synthetase: identification of RNA-binding residues and functional implications for tandem repeats. *Biochemistry* **39**, 15775–15782 (2000).
8. Hirakata, M. *et al*. Autoantibodies to glycyl-transfer RNA synthetase in myositis. Association with dermatomyositis and immunologic heterogeneity. *Arthritis Rheum.* **39**, 146–151 (1996).
9. Lemaire, G., Gros, C., Epely, S., Kaminsky, M. & Labouesse, B. Multiple forms of tryptophanyl-tRNA synthetase from beef pancreas. *Eur. J. Biochem.* **51**, 237–252 (1975).
10. Sallafranque, M.L. *et al*. Tryptophanyl-tRNA synthetase is a major soluble protein species in bovine pancreas. *Biochem. Biophys. Acta* **882**, 192–199 (1986).
11. Favorova, O.O., Zargarova, T.A., Rukosuyev, V.S., Beresten, S.F. & Kisselev, L.L. Molecular and cellular studies of tryptophanyl-tRNA synthetases using monoclonal antibodies: remarkable variations in the content of tryptophanyl-tRNA synthetase in the pancreas of different mammals. *Eur. J. Biochem.* **184**, 583–588 (1989).
12. Kisselev, L.L. Mammalian tryptophanyl-tRNA synthetases. *Biochimie* **75**, 1027–1039 (1993).
13. Wakasugi, K. & Schimmel, P. Two distinct cytokines released from a human aminoacyl-tRNA synthetase. *Science* **284**, 147–151 (1999).
14. Wakasugi, K. *et al*. Induction of angiogenesis by a fragment of human tyrosyl-tRNA synthetase. *J. Biol. Chem.* **277**, 20124–20126 (2002).
15. Tolstrup, A.B., Bejder, A., Fleckner, J. & Justesen, J. Transcriptional regulation of the interferon-γ-inducible tryptophanyl-tRNA synthetase induces alternative splicing. *J. Biol. Chem.* **270**, 397–403 (1995).
16. Wakasugi, K. *et al*. Human aminoacyl-tRNA synthetase as a regulator of angiogenesis. *Proc. Natl. Acad. Sci. USA* **99**, 173–177 (2002).
17. Kisselev, L., Frolova, L. & Haenni, A. L. Interferon inducibility of mammalian tryptophanyl-tRNA synthetase: new perspectives. *Trends Biochem. Sci.* **18**, 263–267 (1993).
18. Shaw, A.C. *et al*. Mapping and identification of interferon gamma-regulated HeLa cell proteins separated by immobilized pH gradient two-dimensional gel electrophoresis. *Electrophoresis* **20**, 984–993 (1999).
19. Otani, A. *et al*. A fragment of human TrpRS as a potent antagonist of ocular angiogenesis. *Proc. Natl. Acad. Sci. USA* **99**, 178–183 (2002).
20. Ewalt, K.L. & Schimmel, P. Activation of angiogenic signaling pathways by two human tRNA synthetases. *Biochemistry* **41**, 13344–13349 (2002).
21. Yang, X.L., Skene, R., McRee, D.E. & Schimmel, P. Crystal structure of a human aminoacyl-tRNA synthetase cytokine. *Proc. Natl. Acad. Sci. USA* **99**, 15369–15374 (2002).
22. Yaremchuk, A., Kriklivyi, I., Tukalo, M. & Cusack, S. Class I tyrosyl-tRNA synthetase has a class II mode of cognate tRNA recognition. *EMBO J.* **21**, 3829–3840 (2002).
23. Kobayashi, T. *et al*. Structural basis for orthogonal tRNA specificities of tyrosyl-tRNA synthetases for genetic code expansion. *Nat. Struct. Biol.* **10**, 425–432 (2003).
24. Jia, J. *et al*. Two essential regions for tRNA recognition in *Bacillus subtilis* tryptophanyl-tRNA synthetase. *Biochem. J.* **365**, 749–756 (2002).
25. Raben, N. *et al*. A motif in human histidyl-tRNA synthetase which is shared among several aminoacyl-tRNA synthetases is a coiled-coil that is essential for enzymatic activity and contains the major autoantigenic epitope. *J. Biol. Chem.* **269**, 24277–24283 (1994).
26. Park, S.G. *et al*. Dose-dependent biphasic activity of tRNA synthetase-associating factor, p43, in angiogenesis. *J. Biol. Chem.* **277**, 45243–45248 (2002).
27. Booth, V., Keizer, D.W., Kamphuis, M.B., Clark-Lewis, I. & Sykes, B.D. The CXCR3 binding chemokine IP-10/CXCL10: structure and receptor interactions. *Biochemistry* **41**, 10418–10425 (2002).
28. Romagnani, P. *et al*. Cell cycle-dependent expression of CXC chemokine receptor 3 by endothelial cells mediates angiostatic activity. *J. Clin. Invest.* **107**, 53–63 (2001).
29. Otani, A. *et al*. Bone marrow–derived stem cells target retinal astrocytes and can promote or inhibit retinal angiogenesis. *Nat. Med.* **8**, 1004–1010 (2002).
30. Otwinowski, Z. & Minor, W. Processing of X-ray diffraction data collected in oscillation mode. *Methods Enzymol.* **276**, 307–326 (1997).
31. Weeks, C.M. & Miller, R. The design and implementation of SnB version 2.0. *J. Appl. Crystallogr.* **32**, 120–124 (1999).
32. Collaborative Computational Project, Number 4. CCP4 Suite: programs for protein crystallography. *Acta Crystallogr. D* **50**, 760–763 (1994).
33. Terwilliger, T.C. Maximum-likelihood density modification. *Acta Crystallogr. D* **56**, 965–972 (2000).
34. Jones, T.A., Zou, J.Y., Cowan, S.W. & Kjeldgaard, M. Improved methods for building protein models in electron density maps and the location of errors in these models. *Acta Crystallogr. A* **47**, 110–119 (1991).
35. Brunger, A.T. *et al*. Crystallography & NMR system: a new software suite for macromolecular structure determination. *Acta Crystallogr. D* **54**, 905–921 (1998).